Oxidation of Pt(111) under Near-Ambient Conditions

D. J. Miller, H. Öberg, S. Kaya, H. Sanchez Casalongue, D. Friebel, T. Anniyev, H. Ogasawara, H. Bluhm, L. G. M. Pettersson, and A. Nilsson

Oxidation of Pt(111) under near-ambient conditions

D. J. Miller[1,2], H. Öberg[3], S. Kaya[1,2], H. Sanchez Casalongue[2], D. Friebel[1,2], T. Anniyev[1,2], H. Ogasawara[2], H. Bluhm[4,5], L. G. M. Pettersson[3] and A. Nilsson[1,2,3,*]

[1]*Stanford Institute for Materials and Energy Sciences, SLAC National Accelerator Laboratory, 2575 Sand Hill Rd, Menlo Park, CA 94025 USA*
[2]*Stanford Synchrotron Radiation Lightsource, SLAC National Accelerator Laboratory, 2575 Sand Hill Rd, Menlo Park, CA 94025, USA*
[3]*Department of Physics, AlbaNova University Center, Stockholm University, S-106 91 Stockholm, Sweden*
[4]*Advanced Light Source, Lawrence Berkeley National Lab, Berkeley, CA 94720, USA*
[5]*Chemical Science Division, Lawrence Berkeley National Lab, Berkeley, CA 94720, USA*

Abstract:

The oxidation of Pt(111) at near-ambient O_2 pressures has been followed *in situ* using x-ray photoelectron spectroscopy (XPS) and *ex situ* using x-ray absorption spectroscopy (XAS). Polarization dependent XAS signatures at the O *K*-edge reveal significant temperature- and pressure-dependent changes of the Pt–O interaction. Oxide growth commences via a PtO-like surface oxide that coexists with chemisorbed oxygen, while an ultrathin α-PtO_2 trilayer is identified as the precursor to bulk oxidation. These results have important implications for understanding the chemical state of Pt in catalysis.

26   Surface oxides with markedly different activities than the metallic surface can form

27   under the O_2-rich conditions employed in many Pt-based industrial processes [1],

28   including the electrochemical oxygen reduction reaction (ORR) [2], CO oxidation [3–5]

29   and the Ostwald process [6]. However, surface-sensitive techniques that can distinguish

30   different oxidation states, e.g., electron-based spectroscopies, are mostly incompatible

31   with the elevated O_2 pressures (> 10^{-5} Torr) required to oxidize Pt. Consequently, even

32   though (111)-oriented facets are the most abundant close-packed surfaces on the Pt

33   nanoparticles [7] typically employed in industrial catalysis, oxide growth on Pt(111)

34   remains poorly understood.

35   Exposing Pt(111) to O_2 under ultrahigh vacuum (UHV) conditions yields

36   chemisorbed $p(2 \times 2)$-O domains with an oxygen coverage, θ, at saturation of

37   0.25 ML [8,9]. However, oxygen phases with θ > 0.25 ML can be prepared in UHV

38   either by using reactive oxygen species, e.g., NO_2 [10–12] and atomic oxygen

39   beams [13,14], or by irradiating saturated O_2 adlayers, e.g., with x-rays [15]. In

40   particular, NO_2 yields a network of linear protrusions that was ascribed to a surface-oxide

41   phase with square-planar Pt–O coordination similar to that of bulk PtO [10].

42   The first *in situ* studies of Pt(111) under high O_2 partial pressures employed surface

43   x-ray diffraction (SXRD) [16]. At near-atmospheric O_2 pressures (>380 Torr) and above

44   520 K the formation of O–Pt–O trilayers similar to those found in α-PtO_2 is

45   observed [16]. However, the precursors to the trilayer oxide have not been characterized;

46   in particular, it is unknown whether the PtO-like surface oxide identified in UHV could

47   also form at elevated O_2 pressures, i.e., under conditions approaching those found in

48   heterogeneous catalysis.

49   Using a photoemission system that can operate at near-ambient pressures (P <

50   5 Torr) [17], we have followed the oxidation of Pt(111) by O_2 by means of x-ray

51   absorption (XAS) and x-ray photoelectron (XPS) spectroscopies. With the aid of density

52   functional theory (DFT) simulations, we demonstrate that oxide growth involves phase

53   transitions from chemisorbed O to two different surface oxides whose structures resemble

54   PtO in the initial stages of oxidation and α-PtO_2 at the onset of bulk oxidation.

The experiments were performed at beamline 11.0.2 of the Advanced Light Source (ALS) using the ambient-pressure XPS endstation [17]. Oxygen layers were prepared by dosing a Pt(111) crystal (cleaned using standard procedures [8]) with up to 5 Torr O_2. XPS was performed *in situ*, while Auger-yield XAS was measured after evacuating O_2, i.e., under UHV conditions; XPS confirmed that the oxygen layers were stable during spectral acquisition. DFT calculations [18] using the PBE exchange-correlation functional [19] were performed with the GPAW program [20,21], which is a real-space-grid-based all-electron DFT code implemented in the projector augmented wave [22] (PAW) formalism. XAS spectra were calculated [23] using the half-core-hole transition potential approach [24], as implemented in GPAW [25].

XPS spectra for O/Pt(111) with coverages up to 2.1 ML are shown in Fig. 1. Surface and bulk Pt atoms of adsorbate-free Pt(111) give rise to Pt $4f_{7/2}$ components at 70.5 and 70.9 eV, respectively [8]. The formation of $p(2 \times 2)$-O domains at 1×10^{-5} Torr O_2 and 300 K yields an additional "chemisorbed" Pt $4f_{7/2}$ component at 71.1 eV, an asymmetric O $1s$ structure at 529.7 eV [8,26], and a single XAS peak close to threshold (~529.9 eV) for both in-plane and out-of-plane polarizations [Fig. 2(a)]. As found in Ref. [8], the out-of-plane spectrum is slightly broader and more intense; otherwise, pronounced polarization dependence is not observed. GPAW simulations [Fig. 2(b)] reproduce all salient features of the observed spectra, thus validating the adopted theoretical approach.

With $P(O_2)$ fixed at 0.5 Torr, the coverage rises steadily from 0.4 ML at $T = 300$ K until saturation (1.1 ML) is attained at ~620 K. Other than the disappearance of the surface peak, below 0.6 ML the only discernible change in Pt $4f$ XPS is a slight broadening of the chemisorbed component toward high binding energy (B.E.). The corresponding XAS spectra are qualitatively similar in all respects to those obtained at 0.25 ML and, as in previous experimental [10] and theoretical studies [27,28], are best reproduced by chemisorbed structure models in which the O adatoms occupy fcc sites, i.e., our results support the growth of $p(2 \times 1)$-O domains.

An additional Pt $4f$ feature between 71.6 and 71.7 eV ("4O") grows in above 420 K when $P(O_2) = 0.5$ Torr ($0.6 < \theta < 1.1$ ML). This is accompanied by a ~ -0.2 eV shift of the O $1s$ XPS peak, which, while smaller than the experimental resolution (~0.3 eV), is

85   matched by a comparable shift of the O K-edge absorption threshold, as expected for a
86   system with metallic screening of the core-ionized $O1s^{-1}$ final state. The concomitant
87   observation of strongly polarization-dependent XAS signatures confirms the growth of a
88   chemically distinct new oxygen phase. In particular, we observe an additional high-
89   energy XAS feature that is significantly more pronounced and located ~ +0.7 eV
90   (531.6 eV) higher in energy in the in-plane spectrum.

91   To address whether the "4O" phase could coexist with chemisorbed O, an oxygen
92   layer generated at 0.5 Torr and 570 K ($\theta = 0.8$ ML) was exposed to 2×10^{-8} Torr H_2 [Fig.
93   3(a)]. Removing up to 0.5 ML of this layer suppressed the near-threshold peak of the in-
94   plane XAS spectrum without significantly affecting the high-energy feature; accordingly,
95   the "4O" Pt $4f$ peak attenuates more rapidly than the chemisorbed component [Figs. 3(a)
96   and 3(c)]. We note, however, that the "4O" layers could be removed completely by
97   longer H_2 exposures (> 4 L, 1 L = 1×10^{-6} Torr s). Since the high-energy feature exhibits
98   no energy shift and the XAS spectra of the 0.3 ML H_2-treated oxygen layer and a
99   saturated "4O" layer (1.1 ML) are in good agreement, H_2-induced structural
100   rearrangements cannot explain the attenuation of the near-threshold peak. The high-
101   energy feature is therefore associated exclusively with the "4O" phase, whereas the near-
102   threshold peak can contain an additional chemisorbed contribution. We moreover assign
103   the double-peaked signature of the 0.30 ML H_2-treated layer [Fig. 3(a)] to a nearly pure
104   "4O" phase.

105   The strong polarization dependence of the "4O" XAS spectrum indicates a highly
106   anisotropic ligand field of the surface Pt atoms: simulations of high-coverage (i.e., $\theta >$
107   0.5 ML) all-fcc chemisorbed structures and high-symmetry subsurface configurations
108   (e.g., the tetrahedral hollow located below the on-surface hcp site) fail to reproduce the
109   observed spectra. The "4O" phase exhibits O $1s$ and Pt $4f$ core-level shifts [Δ_O ~ –0.2 eV,
110   Δ_{Pt} ~ +0.7-0.8 eV, measured with respect to $p(2 \times 2)$-O (529.7 eV) and bulk Pt (70.9 eV),
111   respectively] highly comparable to those reported for 1D oxide chains with square-planar
112   Pt–O coordination that form at the step edges of Pt(533) [6] (Δ_{Pt} ~ +0.55-0.65 eV) and
113   Pt(332) [4] (Δ_O ~ –0.2 eV, Δ_{Pt} = +0.45 ± 0.07 eV), indicating that the coordination
114   environment within the "4O" phase could be similar. Accordingly, the "4O" XAS

4

115 signature is qualitatively reproduced using the 1 ML surface-oxide model structure

116 depicted in Fig. 2(b), which comprises extended oxide chains with Pt–O bonds oriented

117 almost parallel (~15°) to the (111) plane. This structure, proposed by Hawkins *et al*. [28],

118 is generated by occupying selected hcp sites between the close-packed oxygen rows of

119 the $p(2 \times 1)$-O phase [28] and represents the most stable 1 ML configuration identified by

120 those authors using a (2×2) supercell.

121 However, the 1 ML structure can be relaxed further by using larger supercells.

122 Indeed, a single oxide stripe adsorbed on a $(2\sqrt{3} \times 4)$ supercell of Pt(111) yields improved

123 agreement with the observed "4O" spectrum [Fig. 2(b)]: the separation between the near-

124 threshold and high-energy in-plane features (2.2 eV) better matches experiment (2.1 eV),

125 while the high-energy shoulder observed in the out-of-plane direction is now reproduced.

126 Additional simulations (not shown) indicate that the reduced peak separation arises from

127 the longer Pt–O bonds of the isolated stripe ($d = 1.95, 2.06$ Å vs. $1.93, 1.96$ Å in the

128 original structure): whereas the stripe can adopt a local configuration resembling bulk

129 PtO ($d = 2.04$ Å), bond lengthening in the 1 ML structure incurs a large energy penalty.

130 The high-energy shoulder in the out-of-plane spectrum arises from the increased tilt of

131 the isolated stripe with respect to the (111) plane (~29° vs. ~15°), which enhances the

132 spectral weight of O $2p$ hybrid orbitals associated with Pt–O σ^* bonds. Although the

133 absence of a superstructure in LEED prevents more detailed structural conclusions, our

134 simulations clearly identify the "4O" phase as a surface oxide comprising square-planar

135 PtO_4 units.

136 Drastic changes in both O $1s$ and Pt $4f$ XPS are observed upon exposure to ~5 Torr

137 O_2 above 720 K ($\theta > 1.1$ ML): the O $1s$ peak broadens and shifts to higher B.E., while the

138 Pt $4f$ spectrum exhibits—in addition to the bulk peak—two broad, similarly intense

139 features at 72.1 and 73.5 eV. The latter component was also observed after exposing

140 Pt(111) to atomic O [13,14] and *ex situ* following reaction with 750 Torr O_2 at

141 900 K [29]; given the 74.1 eV B.E. of bulk α-PtO_2, it is assigned to Pt atoms with six O

142 nearest neighbors. As demonstrated below, these highly oxidized Pt atoms reside within

143 α-PtO_2(0001) trilayers. Assuming that the surface is uniformly covered by these trilayers,

144 a simple argument based on the mismatch between the in-plane lattice constants of α-

145 PtO$_2$ (3.10 Å) and Pt(111) (2.77 Å) leads to an estimate of ~1.3 trilayers when θ =

146 2.1 ML. However, only a weak (1 × 1) structure is observed in LEED, suggesting that the

147 PtO$_2$-like oxide most likely exists as small domains comprising one or two trilayers.

148 The Pt 4f feature at lower B.E. (72.1 eV) is ascribed to Pt atoms at the interface

149 between trilayer and metallic substrate; the smaller Δ_{Pt} arises from both reduced O

150 coordination and more effective metallic screening. The broadened O 1s peak indicates

151 that at least two chemically distinct oxygen species are present. We identify two

152 components at 529.7 and 530.1 eV, which on the basis of screening arguments and the

153 binding energies of chemisorbed O (529.7 eV [8]) and bulk α-PtO$_2$ (530.2 eV [29]) are

154 assigned to O atoms in the lower and upper layers of the trilayer, respectively. While we

155 are unable to identify XAS features associated with adsorbed OH or H$_2$O [30], additional

156 measurements, e.g., using vibrational spectroscopy, are required to completely exclude

157 that termination of the oxide surface by such species contributes to the broadening of the

158 O 1s XPS feature.

159 PtO$_2$-trilayer formation coincides with drastic changes in the polarization dependence

160 of XAS, which indicates large rearrangements of the coordination environment of the

161 surface Pt atoms. Both in-plane and out-of-plane spectra now exhibit a single broad peak

162 centered at 531.5 and 530.8 eV, respectively, which is associated with transitions to

163 unoccupied O 2p–Pt 5d hybrid states. Partial removal of the trilayer oxide using 2 × 10^{-8}

164 Torr H$_2$ did not induce discernible changes in XAS [Fig. 3(b)]; accordingly, the two

165 oxide-derived Pt 4f XPS components attenuate at comparable rates upon H$_2$ exposure

166 [Fig. 3(d)]. Similar behavior was observed for the trilayer oxide that forms on

167 Rh(111) [31] and clearly indicates that a single phase of oxidic Pt is present beyond

168 1.1 ML. XAS simulations of a single trilayer on Pt(111) are shown in Fig. 2(b). The

169 simulations predict a single peak near-threshold that is shifted to higher energy (~

170 +0.4 eV) in the in-plane spectrum, which agrees well with the observed +0.6 eV shift. We

171 therefore propose that the Pt coordination environment within the surface oxide generated

172 at 2.1 ML resembles the octahedral ligand field of bulk α-PtO$_2$.

173 In summary, beyond a critical chemisorbed coverage of ~0.50 ML the oxidation of

174 Pt(111) proceeds via a PtO-like surface-oxide phase, followed by PtO$_2$-like trilayers that

175   could nucleate at steps or defects [32]. A comparison with oxide growth on other 4*d* and

176   5*d* Pt-group metals is instructive. Pd(111) also forms a surface oxide, Pd_5O_4, that coexists

177   with chemisorbed O [33], but at oxygen chemical potentials much lower than those

178   required to generate the PtO-like phase. This suggests that there is a greater kinetic

179   hindrance to Pt oxidation, which could be associated with the larger cohesion energy of

180   Pt (−5.84 eV) compared to Pd (−3.89 eV); that PtO-like oxide chains form on the more

181   open (2×1)-Pt(110) surface already at 355 K and ~0.01 Torr supports this

182   interpretation [34,35]. Interestingly, whereas the ultrathin trilayer oxide identified on

183   Pt(111) is preceded by a PtO-like surface oxide, analogous oxidic precursors to the

184   trilayer phases that form on Rh(111) [31,36] and Ir(111) [37] have not been found; the

185   elevated temperatures required to initiate bulk-oxide growth on all three surfaces suggest,

186   however, that the trilayer phase passivates the surface against further oxidation.

187   The role of the Pt surface oxides identified here in heterogeneous catalysis should be

188   considered when optimizing the size distribution, morphology, alloy composition and

189   core–shell structure of novel catalysts. Indeed, it was recently shown that the

190   electrochemical oxidation of Pt(111) could also proceed via a PtO-like surface oxide [2]

191   that is associated with a significant activation barrier for oxide reduction and that could,

192   in turn, be responsible for the overpotential of Pt-promoted ORR. This result accords

193   with the observation that the square-planar surface oxide reacts much less readily with

194   hydrogen than does chemisorbed oxygen [see Fig. 3(a)]: understanding oxide-related

195   degradation processes could therefore be critical for obtaining efficient and robust

196   catalysts for fuel-cell applications [2,38].

7

205 *nilsson@slac.stanford.edu

206

207 See Supplemental Material at [*URL to be inserted*] for additional details regarding the

208 experimental setup and for a description of complementary XAS simulations performed

209 using the FEFF8.4 code.

210

211 REFERENCES

212 [1] E. Lundgren *et al.*, J. Phys.: Condens. Matter **18**, R481 (2006).

213 [2] D. Friebel *et al.*, Phys. Chem. Chem. Phys. **13**, 262 (2011).

214 [3] M. D. Ackermann *et al.*, Phys. Rev. Lett. **95**, 255505 (2005).

215 [4] J. G. Wang *et al.*, Phys. Rev. Lett. **95**, 256102 (2005).

216 [5] A. L. Gerrard and J. F. Weaver, J. Chem. Phys. **123**, 224703 (2005).

217 [6] S. Günther *et al.*, J. Phys. Chem. C **112**, 15382 (2008).

218 [7] N. Seriani and F. Mittendorfer, J. Phys.: Condens. Matter **20**, 184023 (2008).

219 [8] C. Puglia *et al.*, Surf. Sci. **342**, 119 (1995).

220 [9] D. J. Miller *et al.*, J. Chem. Phys. **133**, 224701 (2010).

221 [10] S. P. Devarajan, J. A. Hinojosa Jr., and J. F. Weaver, Surf. Sci. **602**, 3116 (2008).

222 [11] R. Getman *et al.*, Phys. Rev. Lett. **102**, 076101 (2009).

223 [12] D. H. Parker, M. E. Bartram, and B. E. Koel, Surf. Sci. **217**, 489 (1989).

224 [13] C. R. Parkinson, M. Walker, and C. F. McConville, Surf. Sci. **545**, 19 (2003).

225 [14] J. F. Weaver, J. J. Chen, and A. L. Gerrard, Surf. Sci. **592**, 83 (2005).

226 [15] Y. S. Kim *et al.*, J. Chem. Phys. **133**, 034501 (2010).

227 [16] C. Ellinger *et al.*, J. Phys.: Condens. Matter **20**, 184013 (2008).

228   [17]   D. F. Ogletree *et al.*, Rev. Sci. Instrum. **73**, 3872 (2002).

229   [18]   Chemisorbed (oxide) slabs comprise four (five) atomic layers of Pt(111), two of
230   them fully relaxed, separated by 14 Å (15 Å) of vacuum and supporting O on one side,
231   see Ref. [9]. ($\sqrt{3} \times 2$) surface cells were used for all slabs except the oxide stripe, for
232   which a ($2\sqrt{3} \times 4$) cell was used. For α-PtO$_2$/Pt(111), we assumed coincidence between
233   ($\sqrt{3} \times \sqrt{3}$)$R30°$ and (2×2) cells of the α-PtO$_2$(0001) trilayer and Pt(111), respectively.
234   This structure was optimized using computed spectra rather than the total energy, since
235   the neglect of van der Waals forces causes uncertainty in the vertical displacement, d_z, of
236   the Pt atoms in the trilayer from the topmost substrate layer. Varying d_z from 2.9 to 4.1 Å
237   while keeping Pt–O distances within the trilayer fixed yielded an optimal d_z of 3.5 Å.

238   [19]   J. P. Perdew, K. Burke, and M. Ernzerhof, Phys. Rev. Lett. **77**, 3865 (1996).

239   [20]   J. Enkovaara *et al.*, J. Phys.: Condens. Matter **22**, 253202 (2010).

240   [21]   J. J. Mortensen, L. B. Hansen, and K. W. Jacobsen, Phys. Rev. B **71**, 035109
241   (2005).

242   [22]   P. E. Blöchl, Phys. Rev. B **50**, 17953 (1994).

243   [23]   PAW setups containing a half core-hole at the excited O were employed. The
244   XAS cross-section was obtained using the Haydock recursion scheme [R. Haydock *et al.*,
245   J. Phys. C: Solid State Phys. **5**, 2845-2858 (1972)] with 2000 Lanczos vectors to avoid
246   explicitly constructing the unoccupied states. The periodic boundary conditions
247   necessitated large supercells ($15 \times 15 \times 30$ Å^3) to eliminate core-hole interactions
248   between adjacent cells.

249   [24]   L. Triguero, L. G. M. Pettersson, and H. Ågren, Phys. Rev. B **58**, 8097 (1998).

250   [25]   M. P. Ljungberg, J. J. Mortensen, and L. G. M. Pettersson, J. Electron Spectrosc.,
251   in press, doi:10.1016/j.elspec.2011.05.004.

9

252   [26]   The high-binding-energy tail of the O 1s feature arises from shake-up excitations

253   rather than from OH and H_2O species, which desorb from metallic Pt well below

254   300 K [8,30].

255   [27]   R. B. Getman, Y. Xu, and W. F. Schneider, J. Phys. Chem. C **112**, 9559 (2008).

256   [28]   J. M. Hawkins, J. F. Weaver, and A. Asthagiri, Phys. Rev. B **79**, 125434 (2009).

257   [29]   M. Peuckert and H. P. Bonzel, Surf. Sci. **145**, 239 (1984).

258   [30]   T. Schiros *et al.*, J. Phys. Chem. C **111**, 15003 (2007).

259   [31]   J. Klikovits *et al.*, J. Phys. Chem. B **110**, 9966 (2006).

260   [32]   S. A. Krasnikov *et al.*, Nanotechnology **21**, 335301 (2010).

261   [33]   E. Lundgren *et al.*, Phys. Rev. Lett. **88**, (2002).

262   [34]   W. X. Li *et al.*, Phys. Rev. Lett. **93**, 146104 (2004).

263   [35]   S. Helveg *et al.*, Surf. Sci. **430**, L533–L539 (1999).
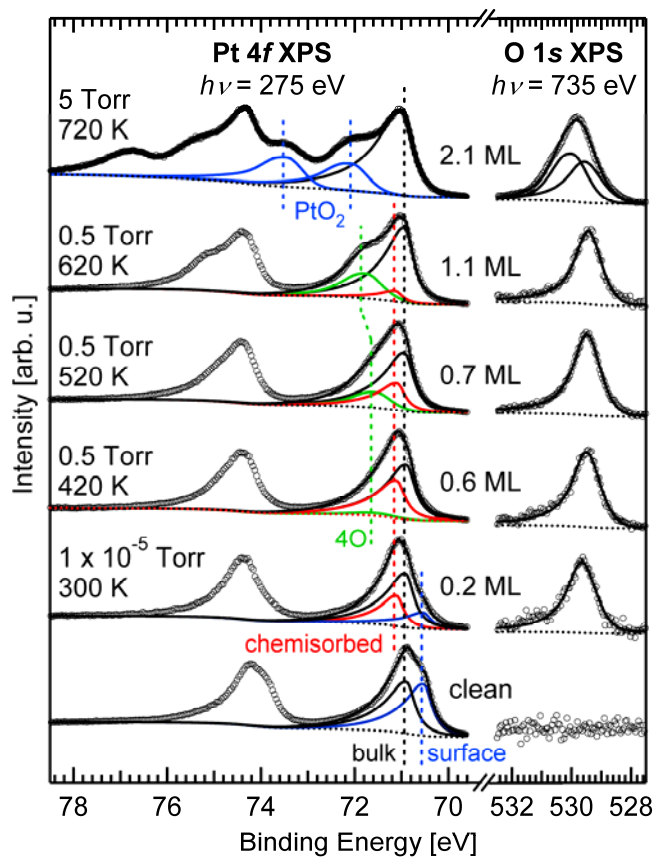
264   [36]   J. Gustafson *et al.*, Phys. Rev. Lett. **92**, 126102 (2004).

265   [37]   Y. B. He *et al.*, J. Phys. Chem. C **112**, 11946-11953 (2011).

266   [38]   D. Friebel *et al.*, Angew. Chem. Int. Ed., in press, doi:10.1002/anie.201101620.
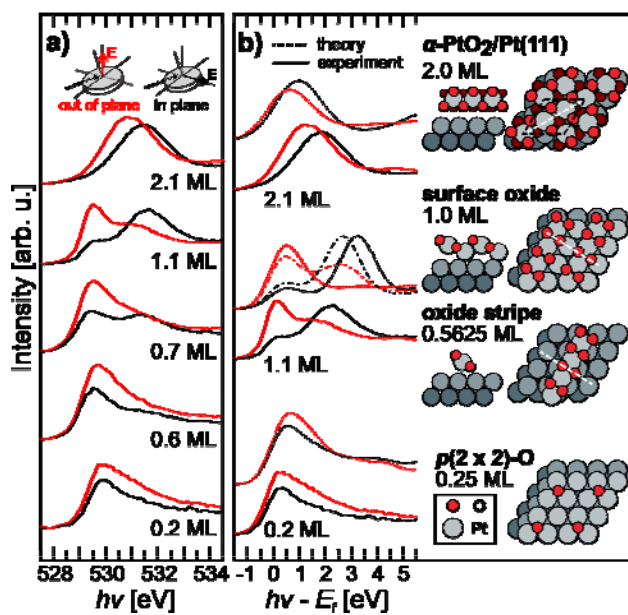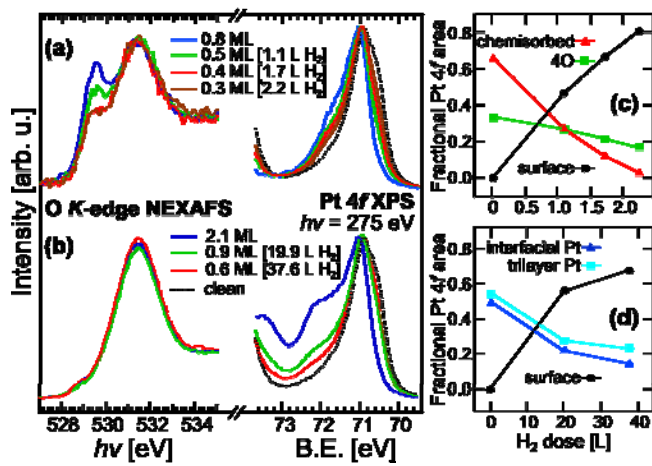
267

271   FIGURE 2

273   FIGURE 3

274

275 FIGURE CAPTIONS

276 FIG. 1 (color online). Pt 4f (left) and O 1s (right) XPS spectra for O/Pt(111),
277 deconvoluted using asymmetric Voigt and Gaussian-broadened Doniach-Šunjić
278 functions, respectively; a Shirley-type background (dashed line) was removed from all
279 spectra. Excepting θ = 2.1 ML, which was prepared at [5 Torr, 720 K] but whose
280 spectrum was acquired at [0.5 Torr, 620 K], the same [$P(O_2)$, T] conditions were
281 employed for sample preparation and spectral acquisition.

282

283 FIG. 2 (color online). Experimental O K-edge XAS spectra (solid lines) are shown in (a)
284 and compared in (b) against simulations (dashed) of the adjacent model structures. Side
285 views of the model structures are cross sections along the dashed lines; the dashed
286 rhombus denotes a (2 × 2) supercell of the Pt(111) substrate. Results for the 1.0 ML
287 surface oxide and isolated oxide chain are shown using dashed and dashed-dotted lines,
288 respectively. Simulations were obtained by convoluting the GPAW output with a Gaussian
289 of 0.45 eV full-width at half-maximum (fwhm), except for α-PtO$_2$/Pt(111), for which
290 0.7 eV was used; these widths were determined from the fwhm of the associated O 1s
291 XPS peaks. Experimental spectra reflect removal of background signal from the Pt
292 substrate and were placed on a B.E. scale in (b) by subtracting the O 1s XPS B.E. All
293 spectra are area normalized ~30 eV above threshold.

294

295 FIG. 3 (color online). In-plane O K-edge XAS spectra (left) and Pt 4$f_{7/2}$ XPS spectra
296 (right) obtained after H$_2$ treatment (2 × 10^{-8} Torr H$_2$ at 300 K) of Pt(111) oxidized at (a)
297 0.5 Torr O$_2$ and 570 K (θ = 0.8 ML) and (b) 5 Torr O$_2$ and 720 K (θ = 2.1 ML). XAS
298 spectra are area normalized ~30 eV above threshold. (c) and (d) show the fraction of the
299 total Pt 4f peak area associated with each oxygen phase as obtained by deconvoluting the
300 Pt 4f XPS spectra in (a) and (b), respectively.